A Approximate Inference

This section provides further details on the algorithms introduced in Section 3.1.

A.1 Variational Inference

Variational inference (VI) minimizes the KL divergence [50] between the true posterior $p(\boldsymbol{\theta} \mid \mathcal{D})$ and the approximate posterior $q(\boldsymbol{\theta} \mid \mathcal{D})$ [6]. While the KL divergence cannot be computed by itself, as the true posterior is unknown, it can still be minimized by maximizing the evidence lower bound (ELBO) given the parameter prior $p(\boldsymbol{\theta})$:

$$\text{ELBO} = \mathop{\mathbb{E}}_{\boldsymbol{\theta} \sim q(\boldsymbol{\theta} \mid \mathcal{D})} \left[\log p(\mathcal{D} \mid \boldsymbol{\theta})\right] - \text{KL}\left[q(\boldsymbol{\theta} \mid \mathcal{D}) \,||\, p(\boldsymbol{\theta})\right] \tag{4}$$

Maximizing the ELBO means maximizing the likelihood of the training data, therefore fitting the data well, while staying close to the parameter prior [6].

Bayes By Backprop (BBB). BBB [7] is an application of VI to deep neural network. BBB approximates the parameter posterior with a diagonal Gaussian distribution that cannot model covariances between parameters. The per-parameter means and variances are learned with standard Stochastic Gradient Descent (SGD) [42] using the negative of the ELBO as the loss function. The ELBO by itself is not differentiable as it depends on the randomly chosen parameters. However, the reparameterization trick [44] applies to diagonal Gaussians and allows us to use the negative ELBO as the loss function. Further runtime performance improvements are possible by using the local reparameterization trick [45] or Flipout [88].

While there have been reports of BBB performing well when used on neural networks [7, 86], the current consensus of the research community seems to be that BBB falls short when compared to e.g. ensembles [20, 72, 89], even though it has been shown that the diagonal Gaussian posterior is not significantly less expressive than a posterior that models covariances [18, 20]. In recent years significant work has been done to improve the performance of VI in a deep learning setting. To assess whether these improved algorithms can compete with SOTA Bayesian algorithms, we also evaluate promising improvements on posterior parameterizations (Rank-1 VI, SVGD) and optimization procedures (iVON).

Rank-1 Variational Inference (Rank-1 VI). Rank-1 VI [17] enhances the posterior approximation of BBB by approximating a full-rank covariance matrix with a low-rank approximation. Rank-1 VI learns a diagonal Gaussian distribution over two vectors per layer, whose outer product is then element-wise multiplied to a learned point estimate of the layer's weights. The bias vector is kept as a point estimate. The limited number of additional parameters allows Rank-1 VI to learn a multi-component Gaussian distribution for the two low-rank vectors, which gives Rank-1 VI ensemble-like properties. Rank-1 VI is both less expressive than BBB with the mean field approximation in the sense that it has fewer variational parameters, and is more expressive as it can model covariances between parameters within a layer and can express multi-modality in a limited way.

Improved Variational Online Newton (iVON). The usage of SGD for the optimization of variational parameters is problematic, as these parameters form a complex, non-euclidean manifold [41]. Natural gradient descent (NGD), recently formalized as the Bayesian learning rule [39], exploits this structure to speed up training. VOGN [41, 70] applies NGD to neural networks but has scaling problems, as it requires per-example gradients in minibatch training. iVON, based on the improved Bayesian learning rule [53], no longer has this problem. While iVON still uses the mean-field approximation of BBB, it is expected to converge faster, and, importantly, halves the number of trainable parameters by implicitly learning per-parameter variances.

Stein Variational Gradient Descent (SVGD). SVGD [55] is a non-parametric VI algorithm that does not assume the posterior to be of a particular shape but approximates it with p particles (i.e. point estimates). The particles can be viewed as members of a Deep Ensemble [51], and the use of VI adds a repulsive component to the loss function based on the RBF kernel distance between the parameters of the particles. While this repulsive component can prevent the particles from converging to the same posterior mode, it prohibits the independent training of the particles.

A.2 Other Algorithms

Deep Ensembles. Lakshminarayanan et al. [51] introduce Deep Ensembles that combine the predictions of multiple independently trained neural networks to improve uncertainty estimates. Originally, Deep Ensembles have been seen as a competing approach to Bayesian algorithms [51]. However, ensembles can be considered to be a Bayesian algorithm that approximates the posterior with a sum of delta distributions [89]. We consider all ensembles to be Bayesian: While they are missing the principled posterior approximation approach of VI, basically hoping that the members converge to different posterior modes, the approach results in a posterior approximation that is in many cases better than the approximation of for example BBB (Section 5, [72, 89]).

Ensembles are usually considered SOTA in uncertainty estimation [72, 89]. However, the training time scales linearly in the number of ensemble members. This makes them highly expensive in cases where training a single member is already expensive, such as with large networks, and opens the space for new, cheaper posterior approximations.

Monte Carlo Dropout (MCD). MCD [22] uses dropout [83] to form a Bernoulli distribution over network parameters. The dropout rates are typically not learned, but the dropout units that are present in many network architectures are simply applied during the evaluation of the model. This very cheap posterior approximation has been criticized for not being truly Bayesian [71]. Despite this criticism, it is still widely used, including in practical applications [10]. When the dropout rate is learned, MCD can be considered to implicitly perform VI [21].

Stochastic Weight Averaging-Gaussian (SWAG). SWAG [59] forms its posterior approximations from the parameter vectors that are traversed during the training of a standard neural network. During the last epochs of SGD training, SWAG periodically stores the current parameters of the neural network to build a low-rank Gaussian distribution over model parameters. While SWAG has only a very small performance overhead during training, storing the additional parameters requires a significant amount of additional memory, and sampling parameters from the low-rank Gaussian distribution incurs a performance overhead during evaluation.

Laplace Approximation. The Laplace approximation [57] builds a local posterior approximation from a second-order Taylor expansion around a MAP model. We always use the last-layer Laplace approximation and switch between a full-rank posterior, diagonal posterior, and a Kronecker-factorized posterior [74] depending on the task. In this configuration, the Laplace approximation is the only post-hoc algorithm that we consider: It can be fitted on top of an existing MAP model by performing a single pass on the training dataset.

B Unsigned Calibration Metrics

As mentioned in the main paper (Section 4), a calibrated model makes confident predictions if and only if they will likely be accurate. Based on this definition, we can directly derive a calibration metric for classification models: The expected calibration error (ECE) [28, 66]. In the regression case, neither "accuracy" nor "confidence" are well-defined properties of a prediction. The notion of calibration must therefore be adapted for regression tasks. In addition, the log marginal likelihood is commonly used to jointly evaluate the accuracy and the calibration in regression tasks. See Appendix G.3.2 for details.

Calibrated Classification. In the classification case, each data point has an associated distribution Y over the possible labels. Y represents the inherent aleatoric uncertainty of the label. Given a prediction $\hat{y} = \arg\max_y p(y \mid \boldsymbol{x}, \mathcal{D})$ made with confidence $\hat{p} = \max_y p(y \mid \boldsymbol{x}, \mathcal{D})$, the model is perfectly calibrated if and only if

$$\mathbb{P}\left(\hat{y} = Y \mid \hat{p} = p\right) = p \qquad \forall p \in [0, 1] \tag{5}$$

holds for every data point [12, 28, 66]. Informally speaking, this means that if the model makes 100 predictions with a confidence of 0.8, 80 of these predictions should be correct. The expected difference between the left and the right side of Equation (5) is called the expected calibration error (ECE) of the model:

$$\text{ECE} = \mathop{\mathbb{E}}_{p \sim \mathcal{U}([0,1])} \left[\left| \mathbb{P}\left(\hat{y} = Y \mid \hat{p} = p\right) - p \right| \right] \tag{6}$$

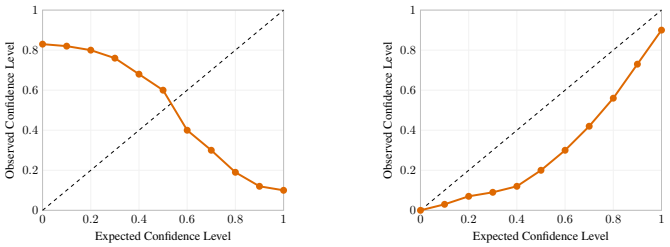

(a) Overconfident Quantile (b) Overconfident CI

Figure 6: Reliability plots of fictional, overconfident regression models when using (a) quantiles and (b) confidence intervals (CI).

It implies two properties of a well-calibrated model: If the accuracy is low, the confidence should also be low. This means that the model must not be overconfident in its predictions. Conversely, if the accuracy is high, the confidence should also be high, meaning that the model must not be underconfident in its predictions.

In practice, a model does not make enough predictions of the same confidence to calculate the calibration error exactly. Therefore, the model's predictions on an evaluation set $\mathcal{D}'$ are commonly grouped into M equally spaced bins B_m based on their confidence values, and the average accuracy and confidence of each bin are used to calculate the ECE [28, 66]:

$$\text{ECE} \approx \sum_{m=1}^{M} \frac{|B_m|}{|\mathcal{D}'|} |\text{acc}(B_m) - \text{conf}(B_m)|, \tag{7}$$

where B_m is the set of predictions in the m-th bin, and $\text{acc}(B_m)$ and $\text{conf}(B_m)$ are the average accuracy and confidence of the predictions in B_m:

$$\text{acc}(B_m) = \frac{1}{|B_m|} \sum_{(\boldsymbol{x},y)\in B_m} \mathbf{1}\big(y = \arg\max_{y'} p(y' \mid \boldsymbol{x}, \mathcal{D})\big) \tag{8}$$

$$\text{conf}(B_m) = \frac{1}{|B_m|} \sum_{(\boldsymbol{x},y)\in B_m} \max_{y'} p(y' \mid \boldsymbol{x}, \mathcal{D}) \tag{9}$$

$$\tag{10}$$

An ECE of zero indicates perfect calibration. We always use ten bins ($M = 10$).

A main problem of the ECE is that bins with few predictions in them may exhibit a high variance [69]. Therefore, Nixon et al. [69] proposed an extension of the ECE that uses bins of adaptive width.

Calibrated Regression. The confidence intervals of the predictive distribution can be used to measure the calibration of a *regression* model [49]. The probability of the ground-truth output $\boldsymbol{y}$ laying inside of the ρ-confidence interval of the predictive distribution of the model for input $\boldsymbol{x}$ should be exactly ρ. Formally, we say a regression model is perfectly calibrated on an evaluation dataset $\mathcal{D}'$ if and only if

$$\mathbb{P}(Q_{\rho'}(\boldsymbol{x}) \leq \boldsymbol{y} \leq Q_{1-\rho'}(\boldsymbol{x})) = \rho \qquad \forall (\boldsymbol{x}, \boldsymbol{y}) \in \mathcal{D}' \tag{11}$$

holds for every q-quantile $Q_q(\boldsymbol{x})$ of the predictive distribution for input $\boldsymbol{x}$ with $\rho' = {}^{(1-\rho)}/_{2}$.

Selectively evaluating Equation (11) for M confidence values ρ_m allows the practical computation of a quantile calibration error (QCE) on an evaluation dataset $\mathcal{D}'$

$$\text{QCE} = \frac{1}{M} \sum_{m=1}^{M} |(\rho_m - p_{\text{obs}}(\rho_m))| \tag{12}$$

with

$$p_{\text{obs}}(\rho_m) = \frac{1}{|\mathcal{D}'|} \sum_{(\boldsymbol{x},\boldsymbol{y})\in\mathcal{D})} \mathbf{1}(Q_{\rho'}(\boldsymbol{x}) \leq \boldsymbol{y} \leq Q_{1-\rho'}(\boldsymbol{x})). \tag{13}$$

The QCE simply replaces the quantiles in the definition of the calibration error from Kuleshov et al. [49] by confidence intervals. Using the confidence intervals allows a simpler interpretation of the resulting reliability diagrams: With the calibration error proposed by Kuleshov et al. [49], the reliability diagram of a perfectly calibrated regression model is a horizontally mirrored version of the reliability diagram of a perfectly calibrated classification model, as there are too many ground-truth values below the lower quantiles of their predictive distributions, and too few above the higher quantiles (Figure 6a). Using confidence intervals for the reliability diagram results in a plot that can be interpreted in the same way as a reliability diagram of a classification model (Figure 6b). We always use ten equally-spaced confident levels between 0 and 1 ($M = 10$).

C Signed Calibration Metrics

As described in the main paper, our signed calibration metrics (sECE and sQCE) may be zero even though the model is not perfectly calibrated. However, we show that this is typically not an issue in practice, as for most models nearly all predictions are overconfident or nearly all predictions are underconfident. The reliability diagrams in Figure 7 confirm this for a representative selection of overconfident and underconfident models. We always report the unsigned calibration metrics in Appendix G in addition to the signed calibration metrics mentioned in the main paper. The unsigned metrics are in almost all cases very close to the absolute value of the signed metric, resulting in the same relative ordering of the algorithms. On the other hand, the sECE provides valuable insights into the underconfidence of some algorithms such as MultiSWAG on CIFAR-10 and SWAG on AMAZON-WILDS.

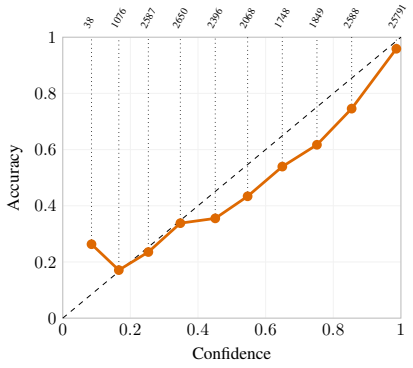

(a) MAP on the o.o.d. evaluation split of iWildCam-wilds. sECE: −0.0457, ECE: 0.0463

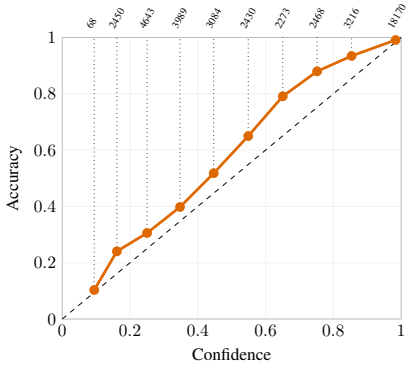

(b) MultiLaplace on the o.o.d. evaluation split of iWildCam-wilds. sECE: −0.04501, ECE: 0.0501

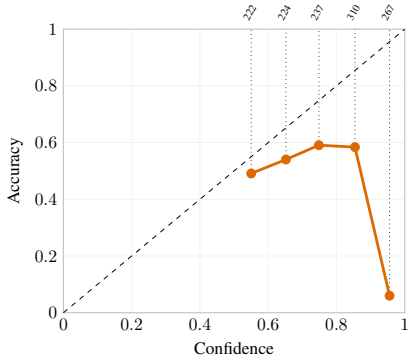

(c) MAP on the group with the worst accuracy on CivilComments-wilds. sECE: −0.3162, ECE: 0.3162

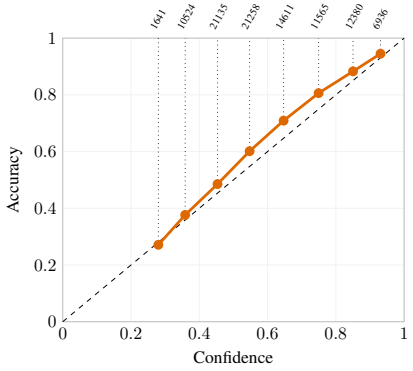

(d) SWAG on the o.o.d. evaluation split of Amazon-wilds. sECE: −0.0405, ECE: 0.0408

Figure 7: Reliability diagrams of different models on a variety of datasets. No data point is drawn for empty bins. The number of predictions in each bin is denoted at the top of each plot. The dashed line corresponds to a perfectly calibrated model. In all cases, either nearly all of the model's predictions are overconfident, or nearly all are underconfident. Therefore, the ECE is close to the absolute value of the sECE, indicating that the sECE is a reasonable calibration metric.

D Implementation Details

Except for Laplace, we implement all algorithms ourselves as PyTorch [24] optimizers. The implementation of the algorithms as well as code to reproduce all experiments is available at `https://github.com/bdl-authors/beyond-ensembles`, where we also provide a short tutorial on the usage of our implementation.

Bayes By Backprop. We use the local reparameterization trick [45]. As it is standard today [20, 72, 89], we do not use the scale mixture prior introduced by BBB's original authors [7], but a unit Gaussian prior. For the experiments on CIFAR-10, we make the parameters of the Filter Response Normalization layers variational.

Rank-1 VI. Following Dusenberry et al. [17], we keep the bias of each layer as a point estimate. We also keep the learned parameters of batch normalization and Filter Response Normalization layers as point estimates. We use five components in most cases which is close to the four components recommended by Dusenberry et al. [17] and make Rank-1 VI directly comparable to other ensemble-based models that use five members.

iVON. We adapt the data augmentation factor that Osawa et al. [70] introduce for VOGN [40] to iVON. We do not use the tempering parameter from VOGN.

Laplace. We use the Laplace library from Daxberger et al. [13] due to the difficulty of implementing second-order optimization in PyTorch. In all cases except for CIVILCOMMENTS-WILDS, we use a Kronecker-factorized last-layer Laplace approximation. On CIVILCOMMENTS-WILDS, we use a diagonal last-layer Laplace approximation as the Kronecker-factorized approximation frequently leads to diverging parameters. We do not use the GLM approximation as proposed by Daxberger et al. [13] but use Monte Carlo sampling to stay consistent with the other evaluated algorithms. In all experiments we use the Laplace library's functions to tune the prior precision after fitting the Laplace approximation.

SWAG. While the authors of SWAG argue that SWAG benefits from a special learning rate schedule [59], they do not use such a schedule in most of their experiments with SWAG and MultiSWAG [89]. Correspondingly, we use the same schedule with SWAG as with any other algorithm. We use 30 parameter samples for building the mean and the low-rank covariance matrix of SWAG. On CIVILCOMMENTS-WILDS, we only use 10 parameter samples due to the storage size of the samples.

E Batch Normalization, Distribution Shift, and Bayesian Deep Learning

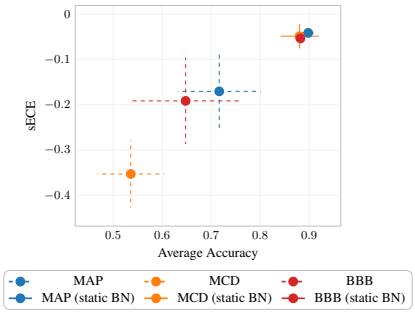

Figure 8: CAMELYON17-WILDS: Average accuracy vs. sECE on the o.o.d. test split. The models that use no running statistics (static BN) are significantly more accurate and better calibrated, while exhibiting a smaller variance.

Schneider et al. [77] find that a significant part of the accuracy loss on o.o.d. data is due to changing batch statistics that cannot be adequately normalized by the running batch normalization statistics that are based on the training data. The authors propose to re-initialize the running statistics on a subset of the evaluation dataset.

We are able to reproduce the issue with o.o.d. data on the CAMELYON17-WILDS dataset from the WILDS collection [47] (Figure 8). The o.o.d. evaluation set of CAMELYON17 has been generated by selecting the images that were most visually distinct from the other images. In addition, the employed ResNet-20 [32] architecture includes batch normalization layers. We find that using only batch statistics, thereby essentially using the batch normalization layers in training mode during evaluation, entirely alleviates the i.d. - o.o.d. performance gap on CAMELYON17, as well as the large standard deviations on the o.o.d. dataset. Coincidentally, the WILDS leaderboard [46] shows that models that do not include batch normalization, such as a model based on the vision transformer [15], or that use extensive data augmentation, perform best.

The running statistics of batch normalization layers also pose problems with Bayesian neural networks that sample parameters, as the running statistics depend on the parameters of the neural network. Wilson and Izmailov [89] therefore propose to recalculate the batch normalization statistics for each parameter sample. This is not necessary in our case as we never use running statistics for normalization layers. By doing so we also avoid the aforementioned distribution-shift problem without requiring additional o.o.d. data during evaluation, and do not add any computation overhead.

F Computational Resources

We use single NVIDIA Tesla V100, A100, and H100 GPUs for all tasks from Wilds [47] and CIFAR-10-(C) [33, 48]. See Table 1 for the GPUs that we use on the individual datasets as well as the runtime of MAP. Table 2 displays the relative runtime of the BDL algorithms. In total, we estimate that the evaluation required about $1600\,\mathrm{h}$ of GPU time, of which about 25% were consumed during implementation, testing and hyperparameter optimization. Training and hyperparameter optimization of the UCI models was performed on a single CPU in about $20\,\mathrm{h}$. Table 3 shows the GPU memory overhead of the BDL algorithms.

Dataset	GPU	Runtime of MAP
CIFAR-10	NVIDIA V100	50 min
PovertyMap-wilds	NVIDIA V100	50 min
iWildCam-wilds	NVIDIA A100	150 min
FMoW-wilds	NVIDIA V100	150 min
RxRx1-wilds	NVIDIA V100	140 min
CivilComments-wilds	NVIDIA A100	60 min
Amazon-wilds	NVIDIA H100	90 min

Table 1: Hardware and runtime for MAP for each dataset. The results are rounded to the next 10 minutes.

Model	PovertyMap	iWildCam	FMoW	RxRx1	CivilComments	Amazon	CIFAR-10
MAP	1.0	1.0	1.0	1.0	1.0	1.0	1.0
MCD	1.0	1.0	1.0	1.0	1.0	1.0	~ 1.0
SWAG	1.3	1.5	1.0	1.2	1.3	1.5	~ 1.0
Laplace	1.0	1.0	1.0	1.0	1.0	1.0	~ 1.0
BBB	5.7	-	-	-	-	-	~ 5.0
LL BBB	-	1.6	2.0	3.7	1.8	2.0	-
Rank-1 VI	3.9	-	-	-	-	-	~ 4.0
LL Rank-1 VI	-	2.0	2.0	3.7	1.9	2.0	-
iVON	2.8	-	-	-	-	-	~ 3.0
LL iVON	-	3.0	2.9	3.6	5.6	6.6	-
SVGD	9.2	4.9	7.3	8.9	9.2	10.0	~ 8.0

Table 2: Runtime of different algorithms relative to MAP. The numbers on CIFAR-10 are conservative estimates as exact numbers were no longer available. Note that the runtime also depends on whether we are able to use mixed precision training, which was not possible with the VI algorithms. The training time of a MultiX model with n members is n times the training time of the respective single-mode approximation. LL = Last-Layer.

Model	Memory Overhead
MAP	1.0
MCD	1.0
SWAG	~ 1.0
Laplace	~ 1.0
BBB	~ 2
Rank-1 VI	$\sim 1 + \#\text{components} \cdot \sqrt{\text{parameter count}}$
iVON	~ 2[5]
SVGD	$\sim \#\text{particles}$

Table 3: GPU memory requirements of different algorithms relative to MAP. The numbers are estimates are based on a theoretical analysis of the algorithms, not on measurements. The memory consumption of MultiX is the same as for the respective single-mode approximation, since all members can be trained indenpendently.

[5] No additional memory overhead due to a separate optimizer

G Additional Experimental Results

G.1 UCI Datasets

We report results for both the standard and the gap splits [20] on the HOUSING and ENERGY datasets from the UCI machine learning repository [16]. On ENERGY, we can reproduce the catastrophic failure of VI both with BBB and Rank-1 VI, but not with iVON which performs still similarly to MultiSWAG. Overall, we find that the benefit of ensembles is less clear than on the larger WILDS datasets, which emphasizes the importance of evaluating Bayesian algorithms on large datasets.

Hyperparameters. All hyperparameters were optimized through a grid search on the validation set. Note that for the gap splits the validation set is not part of the gap. We considered 40, 100 and 200 epochs, learning rates of 0.01 and 0.001 and (where applicable) weight decay factors of 10^{-4} and 10^{-5}. For BBB, the prior standard deviations are 0.1, 1.0 and 10.0 and we scale the KL divergence in the ELBO by 0.2, 0.5, and 1.0, with colder temperatures generally leading to better results. For iVON, we consider prior precisions of 10, 100, and 200, with 200 being selected in most cases. BBB and iVON use five Monte Carlo samples during training. For SWAG, we consider 60, 100, and 150 epochs, use 30 parameter samples and start sampling after 50%, 75%, or 90% of the training epochs were completed. For Laplace, we always use a last-layer approximation with a full covariance matrix. We use the Adam optimizer [43] to optimize the log-likelihood/ELBO and learn the output standard deviation jointly with the parameters. We use 1000 parameter samples for each prediction.

Model	LML	MSE	QCE	sQCE
MAP	-2.643 ± 0.054	10.707 ± 0.794	$\mathbf{0.036 \pm 0.001}$	$\mathbf{-0.018 \pm 0.012}$
Deep Ensemble	$\mathbf{-2.330 \pm 0.015}$	6.034 ± 0.413	0.099 ± 0.006	0.099 ± 0.006
MCD	-2.836 ± 0.095	13.531 ± 1.401	0.044 ± 0.008	-0.031 ± 0.019
MultiMCD	$\mathbf{-2.328 \pm 0.010}$	$\mathbf{5.789 \pm 0.077}$	0.101 ± 0.002	0.101 ± 0.002
SWAG	-2.495 ± 0.014	6.044 ± 0.214	0.128 ± 0.003	0.128 ± 0.003
MultiSWAG	-2.511 ± 0.002	7.071 ± 0.011	0.139 ± 0.002	0.139 ± 0.002
LL Laplace	-2.515 ± 0.058	9.498 ± 2.347	0.099 ± 0.020	0.099 ± 0.020
LL MultiLaplace	-2.467 ± 0.031	$\mathbf{5.850 \pm 0.395}$	0.157 ± 0.005	0.157 ± 0.005
BBB	-2.475 ± 0.096	7.716 ± 1.053	$\mathbf{0.033 \pm 0.004}$	$\mathbf{-0.006 \pm 0.012}$
MultiBBB	-2.529 ± 0.003	7.212 ± 0.160	0.172 ± 0.005	0.172 ± 0.005
Rank-1 VI	-2.531 ± 0.103	8.983 ± 1.451	$\mathbf{0.033 \pm 0.008}$	$\mathbf{0.006 \pm 0.016}$
iVON	-2.793 ± 0.006	9.853 ± 0.318	0.215 ± 0.003	0.215 ± 0.003
SVGD	-2.614 ± 0.017	8.397 ± 0.642	0.143 ± 0.010	0.143 ± 0.010

Table 4: UCI-HOUSING (standard splits)

Model	LML	MSE	QCE	sQCE
MAP	-2.850 ± 0.207	14.775 ± 3.635	$\mathbf{0.040 \pm 0.013}$	$\mathbf{-0.012 \pm 0.024}$
Deep Ensemble	-2.767 ± 0.183	$\mathbf{13.012 \pm 3.034}$	0.054 ± 0.011	0.045 ± 0.017
MCD	-2.892 ± 0.210	15.488 ± 3.661	$\mathbf{0.034 \pm 0.007}$	$\mathbf{-0.001 \pm 0.018}$
MultiMCD	$\mathbf{-2.730 \pm 0.132}$	$\mathbf{12.760 \pm 2.838}$	0.054 ± 0.013	0.045 ± 0.019
SWAG	-2.743 ± 0.042	$\mathbf{12.940 \pm 1.742}$	0.113 ± 0.017	0.112 ± 0.017
MultiSWAG	$\mathbf{-2.694 \pm 0.047}$	$\mathbf{11.941 \pm 1.874}$	0.118 ± 0.020	0.117 ± 0.020
LL Laplace	-2.873 ± 0.117	15.294 ± 3.687	0.074 ± 0.018	0.072 ± 0.020
LL MultiLaplace	-2.832 ± 0.106	$\mathbf{13.445 \pm 3.209}$	0.106 ± 0.020	0.104 ± 0.022
BBB	-3.829 ± 1.009	17.238 ± 7.435	0.114 ± 0.024	-0.113 ± 0.024
MultiBBB	$\mathbf{-2.734 \pm 0.115}$	14.071 ± 2.925	0.065 ± 0.018	0.054 ± 0.026
Rank-1 VI	-2.806 ± 0.193	$\mathbf{13.513 \pm 2.930}$	0.067 ± 0.025	$\mathbf{0.018 \pm 0.043}$
iVON	-2.930 ± 0.023	17.904 ± 2.300	0.152 ± 0.015	0.151 ± 0.015
SVGD	-2.855 ± 0.184	14.848 ± 3.170	$\mathbf{0.039 \pm 0.014}$	$\mathbf{-0.003 \pm 0.025}$

Table 5: UCI-HOUSING (gap splits)

Model	LML	MSE	QCE	sQCE
MAP	-1.702 ± 0.094	1.760 ± 0.289	$\mathbf{0.051 \pm 0.020}$	$\mathbf{-0.020 \pm 0.036}$
Deep Ensemble	-1.235 ± 0.003	$\mathbf{0.177 \pm 0.007}$	0.270 ± 0.002	0.270 ± 0.002
MCD	-1.709 ± 0.079	1.779 ± 0.252	$\mathbf{0.049 \pm 0.016}$	$\mathbf{-0.022 \pm 0.032}$
MultiMCD	-1.236 ± 0.005	0.212 ± 0.015	0.260 ± 0.003	0.260 ± 0.003
SWAG	-2.127 ± 0.029	2.198 ± 0.274	0.210 ± 0.006	0.210 ± 0.006
MultiSWAG	-2.143 ± 0.002	2.454 ± 0.018	0.220 ± 0.001	0.220 ± 0.001
LL Laplace	-1.653 ± 0.026	0.608 ± 0.110	0.245 ± 0.019	0.245 ± 0.019
LL MultiLaplace	-1.606 ± 0.016	0.235 ± 0.033	0.316 ± 0.008	0.316 ± 0.008
BBB	$\mathbf{-0.976 \pm 0.123}$	0.413 ± 0.103	$\mathbf{0.055 \pm 0.017}$	$\mathbf{0.030 \pm 0.032}$
MultiBBB	$\mathbf{-1.022 \pm 0.021}$	0.309 ± 0.075	0.210 ± 0.012	0.210 ± 0.012
Rank-1 VI	$\mathbf{-1.029 \pm 0.166}$	0.459 ± 0.145	$\mathbf{0.054 \pm 0.019}$	$\mathbf{0.019 \pm 0.036}$
iVON	-2.463 ± 0.006	6.620 ± 0.191	0.161 ± 0.010	0.161 ± 0.010
SVGD	-1.322 ± 0.040	0.550 ± 0.121	0.159 ± 0.027	0.159 ± 0.027

Table 6: UCI-ENERGY (standard splits)

Model	LML	MSE	QCE	sQCE
MAP	-7.723 ± 7.553	$\mathbf{34.444 \pm 41.620}$	0.247 ± 0.065	$\mathbf{0.043 \pm 0.195}$
Deep Ensemble	-4.360 ± 3.066	$\mathbf{31.419 \pm 36.845}$	0.272 ± 0.060	$\mathbf{0.072 \pm 0.207}$
MCD	-10.299 ± 10.685	48.491 ± 58.682	0.261 ± 0.065	$\mathbf{0.041 \pm 0.206}$
MultiMCD	-6.744 ± 6.151	41.030 ± 49.269	0.272 ± 0.061	$\mathbf{0.073 \pm 0.207}$
SWAG	$\mathbf{-3.655 \pm 1.469}$	$\mathbf{30.372 \pm 28.902}$	0.218 ± 0.084	$\mathbf{0.011 \pm 0.183}$
MultiSWAG	$\mathbf{-3.110 \pm 0.815}$	$\mathbf{25.362 \pm 22.428}$	0.192 ± 0.059	$\mathbf{0.034 \pm 0.152}$
LL Laplace	-7.009 ± 4.256	45.505 ± 37.787	0.247 ± 0.040	$\mathbf{0.116 \pm 0.119}$
LL MultiLaplace	-5.549 ± 2.983	38.452 ± 31.657	0.270 ± 0.046	$\mathbf{0.142 \pm 0.127}$
BBB	-64.268 ± 79.182	43.670 ± 52.833	0.199 ± 0.131	$\mathbf{-0.101 \pm 0.184}$
MultiBBB	-22.150 ± 25.068	50.502 ± 58.432	0.236 ± 0.110	$\mathbf{-0.073 \pm 0.202}$
Rank-1 VI	-72.412 ± 92.191	49.099 ± 60.606	0.191 ± 0.133	$\mathbf{-0.109 \pm 0.178}$
iVON	$\mathbf{-3.367 \pm 0.903}$	$\mathbf{21.546 \pm 13.347}$	$\mathbf{0.109 \pm 0.025}$	$\mathbf{0.038 \pm 0.074}$
SVGD	-9.945 ± 10.449	46.757 ± 56.551	0.227 ± 0.067	$\mathbf{0.037 \pm 0.182}$

Table 7: UCI-ENERGY (gap splits)

G.2 CIFAR-10

Following Wilson et al. [90], we train a ResNet-20 [32] with Swish activations [73] and Filter Response Normalization [82]. The use of Filter Response Normalization instead of batch normalization, which only uses batch statistics, eliminates the problems mentioned in Appendix E. We train all models except iVON with SGD and a learning rate of 0.05 and Nesterov momentum of strength 0.9 for 300 epochs. We use the learning rate schedule from Maddox et al. [59]: The learning rate is kept at its initial value for the first 150 epochs, then linearly reduced to a learning rate of 0.005 at epoch 270 at which it is kept constant for the remaining 30 epochs. For MCD, we use a dropout rate of 0.1 and insert dropout units after every linear and convolutional layer of the ResNet-20. For BBB, we temper the KL divergence in the ELBO with a factor of 0.2. Rank-1 VI uses an untempered posterior and four components. BBB and iVON use two Monte Carlo samples during training. The Laplace approximation is based on a diagonal last-layer approximation. iVON is also trained for 300 epochs with a learning rate of $1 \cdot 10^{-4}$, a prior precision of 50, and a data augmentation factor of 10 (see Osawa et al. [70] for details), but uses no learning rate schedule. We found these changes to be necessary to ensure that iVON performs well, likely because iVON is much more similar to Adam [43] than to SGD and therefore needs a smaller learning rate. Following Nado et al. [65], SNGP uses a spectral normalization factor of 6.0 and mean field factor of 20. We did not perform any additional tuning of the mean field factor. We always use 50 parameter samples during evaluation.

Figure 9 displays the accuracy, ECE, sECE, agreement with HMC, and TV compared to HMC. MultiX models tend to become underconfident. Table 8 shows detailed numerical results for all algorithms and corruption levels.

Model	Accuracy	ECE	sECE	NLL	Agreement	TV
MAP	0.925 ± 0.001	0.045 ± 0.001	-0.045 ± 0.001	0.296 ± 0.006	0.906 ± 0.002	0.172 ± 0.001
Deep Ensemble	$\mathbf{0.944 \pm 0.001}$	0.010 ± 0.001	$\mathbf{0.003 \pm 0.000}$	$\mathbf{0.174 \pm 0.001}$	0.923 ± 0.001	0.144 ± 0.001
MCD	0.927 ± 0.002	$\mathbf{0.008 \pm 0.001}$	0.007 ± 0.001	0.216 ± 0.005	0.920 ± 0.003	0.132 ± 0.002
MultiMCD	0.941 ± 0.001	0.031 ± 0.001	0.031 ± 0.001	0.186 ± 0.001	0.930 ± 0.002	0.116 ± 0.001
SWAG	0.921 ± 0.002	0.042 ± 0.003	0.042 ± 0.003	0.250 ± 0.002	0.910 ± 0.002	0.130 ± 0.001
MultiSWAG	0.940 ± 0.001	0.099 ± 0.002	0.099 ± 0.002	0.258 ± 0.002	0.927 ± 0.001	0.107 ± 0.001
LL Laplace	0.924 ± 0.001	0.040 ± 0.001	-0.040 ± 0.001	0.282 ± 0.006	0.906 ± 0.002	0.169 ± 0.001
LL MultiLaplace	$\mathbf{0.945 \pm 0.001}$	0.012 ± 0.002	0.007 ± 0.001	$\mathbf{0.174 \pm 0.002}$	0.923 ± 0.001	0.142 ± 0.000
BBB	0.898 ± 0.003	0.046 ± 0.002	-0.046 ± 0.002	0.387 ± 0.011	0.900 ± 0.001	0.161 ± 0.001
MultiBBB	0.929 ± 0.001	0.018 ± 0.002	0.018 ± 0.002	0.228 ± 0.002	0.930 ± 0.001	0.122 ± 0.001
Rank1-VI	0.881 ± 0.003	0.041 ± 0.002	0.041 ± 0.002	0.363 ± 0.005	0.910 ± 0.003	0.116 ± 0.002
iVON	0.842 ± 0.004	0.025 ± 0.003	0.024 ± 0.003	0.464 ± 0.011	0.874 ± 0.004	0.145 ± 0.003
MultiiVON	0.881 ± 0.003	0.077 ± 0.003	0.077 ± 0.003	0.388 ± 0.002	0.921 ± 0.002	0.107 ± 0.001
SVGD	0.927 ± 0.001	0.018 ± 0.001	$\mathbf{0.003 \pm 0.001}$	0.255 ± 0.001	0.924 ± 0.002	0.135 ± 0.001
SNGP	0.917 ± 0.003	0.076 ± 0.006	0.076 ± 0.006	0.380 ± 0.013	0.903 ± 0.002	0.178 ± 0.002
HMC	0.903	0.069	0.068	0.320	1.000	0.000

(a) Standard Evaluation Split (Corruption Level 0)

Model	Accuracy	ECE	sECE	NLL	Agreement	TV
MAP	0.872 ± 0.002	0.080 ± 0.002	-0.080 ± 0.002	0.518 ± 0.010	0.848 ± 0.001	0.238 ± 0.001
Deep Ensemble	$\mathbf{0.903 \pm 0.001}$	0.014 ± 0.001	$\mathbf{-0.003 \pm 0.001}$	$\mathbf{0.305 \pm 0.006}$	0.870 ± 0.003	0.196 ± 0.001
MCD	0.872 ± 0.004	$\mathbf{0.011 \pm 0.003}$	$\mathbf{-0.004 \pm 0.006}$	0.400 ± 0.011	0.865 ± 0.003	0.184 ± 0.002
MultiMCD	0.890 ± 0.003	0.028 ± 0.002	0.026 ± 0.002	0.335 ± 0.005	0.880 ± 0.002	0.158 ± 0.001
SWAG	0.876 ± 0.004	0.047 ± 0.006	0.047 ± 0.005	0.388 ± 0.004	0.856 ± 0.005	0.179 ± 0.001
MultiSWAG	0.900 ± 0.001	0.117 ± 0.002	0.117 ± 0.002	0.383 ± 0.002	0.878 ± 0.001	0.147 ± 0.000
LL Laplace	0.873 ± 0.004	0.074 ± 0.004	-0.074 ± 0.004	0.499 ± 0.017	0.849 ± 0.002	0.239 ± 0.002
LL MultiLaplace	$\mathbf{0.903 \pm 0.005}$	0.016 ± 0.003	$\mathbf{-0.001 \pm 0.005}$	0.314 ± 0.003	0.859 ± 0.004	0.199 ± 0.001
BBB	0.839 ± 0.003	0.083 ± 0.003	-0.083 ± 0.003	0.682 ± 0.029	0.844 ± 0.002	0.222 ± 0.000
MultiBBB	0.878 ± 0.008	0.018 ± 0.005	0.006 ± 0.009	0.394 ± 0.012	0.880 ± 0.005	0.170 ± 0.004
Rank1-VI	0.843 ± 0.004	0.042 ± 0.004	0.042 ± 0.004	0.484 ± 0.015	0.860 ± 0.002	0.165 ± 0.003
iVON	0.795 ± 0.010	0.025 ± 0.006	0.010 ± 0.010	0.596 ± 0.021	0.827 ± 0.011	0.189 ± 0.008
MultiiVON	0.845 ± 0.004	0.083 ± 0.003	0.081 ± 0.003	0.504 ± 0.018	0.863 ± 0.008	0.145 ± 0.003
SVGD	0.883 ± 0.001	0.021 ± 0.003	-0.007 ± 0.001	0.432 ± 0.010	0.875 ± 0.001	0.192 ± 0.000
SNGP	0.867 ± 0.015	0.074 ± 0.009	0.069 ± 0.012	0.560 ± 0.034	0.844 ± 0.010	0.231 ± 0.004
HMC	0.834	0.066	0.064	0.508	1.000	0.000

(b) Corruption Level 1

Model	Accuracy	ECE	sECE	NLL	Agreement	TV
MAP	0.805 ± 0.005	0.128 ± 0.005	-0.128 ± 0.004	0.863 ± 0.019	0.778 ± 0.002	0.309 ± 0.002
Deep Ensemble	$\mathbf{0.838 \pm 0.004}$	0.027 ± 0.004	-0.027 ± 0.004	$\mathbf{0.518 \pm 0.020}$	0.805 ± 0.002	0.253 ± 0.001
MCD	0.777 ± 0.011	0.047 ± 0.004	-0.047 ± 0.005	0.733 ± 0.051	0.796 ± 0.010	0.232 ± 0.001
MultiMCD	0.805 ± 0.003	$\mathbf{0.011 \pm 0.003}$	$\mathbf{0.000 \pm 0.003}$	0.594 ± 0.012	0.823 ± 0.005	0.196 ± 0.001
SWAG	0.806 ± 0.004	0.032 ± 0.003	0.031 ± 0.004	0.593 ± 0.009	0.783 ± 0.005	0.228 ± 0.003
MultiSWAG	$\mathbf{0.839 \pm 0.002}$	0.117 ± 0.004	0.117 ± 0.004	0.556 ± 0.002	0.818 ± 0.001	0.186 ± 0.001
LL Laplace	0.804 ± 0.003	0.120 ± 0.002	-0.119 ± 0.002	0.839 ± 0.021	0.777 ± 0.005	0.308 ± 0.003
LL MultiLaplace	$\mathbf{0.850 \pm 0.012}$	0.026 ± 0.008	-0.015 ± 0.009	$\mathbf{0.498 \pm 0.035}$	0.800 ± 0.002	0.251 ± 0.003
BBB	0.735 ± 0.009	0.154 ± 0.008	-0.154 ± 0.008	1.296 ± 0.072	0.774 ± 0.004	0.286 ± 0.002
MultiBBB	0.786 ± 0.014	0.033 ± 0.010	-0.026 ± 0.014	0.741 ± 0.045	0.830 ± 0.006	0.204 ± 0.003
Rank1-VI	0.774 ± 0.008	0.024 ± 0.002	0.019 ± 0.006	0.684 ± 0.027	0.802 ± 0.006	0.210 ± 0.005
iVON	0.725 ± 0.014	0.028 ± 0.004	-0.022 ± 0.005	0.809 ± 0.036	0.756 ± 0.016	0.237 ± 0.008
MultiiVON	0.783 ± 0.008	0.069 ± 0.009	0.068 ± 0.010	0.666 ± 0.006	0.821 ± 0.002	0.179 ± 0.003
SVGD	0.804 ± 0.004	0.038 ± 0.002	-0.038 ± 0.002	0.821 ± 0.024	0.818 ± 0.001	0.238 ± 0.001
SNGP	0.785 ± 0.015	0.067 ± 0.007	0.044 ± 0.010	0.837 ± 0.042	0.767 ± 0.008	0.295 ± 0.004
HMC	0.724	0.020	0.017	0.833	1.000	0.000

(c) Corruption Level 3

Model	Accuracy	ECE	sECE	NLL	Agreement	TV
MAP	0.689 ± 0.006	0.217 ± 0.006	-0.217 ± 0.006	1.494 ± 0.019	0.683 ± 0.005	0.390 ± 0.003
Deep Ensemble	$\mathbf{0.733 \pm 0.006}$	0.075 ± 0.007	-0.075 ± 0.007	0.937 ± 0.036	0.718 ± 0.004	0.310 ± 0.003
MCD	0.629 ± 0.009	0.141 ± 0.011	-0.141 ± 0.010	1.312 ± 0.094	0.725 ± 0.012	0.277 ± 0.003
MultiMCD	0.666 ± 0.007	0.069 ± 0.007	-0.069 ± 0.007	1.063 ± 0.021	0.760 ± 0.001	0.234 ± 0.001
SWAG	0.696 ± 0.005	$\mathbf{0.018 \pm 0.009}$	-0.012 ± 0.008	0.927 ± 0.025	0.699 ± 0.006	0.277 ± 0.006
MultiSWAG	$\mathbf{0.728 \pm 0.004}$	0.082 ± 0.004	0.082 ± 0.004	$\mathbf{0.841 \pm 0.009}$	0.740 ± 0.004	0.228 ± 0.002
LL Laplace	0.690 ± 0.006	0.203 ± 0.005	-0.203 ± 0.005	1.430 ± 0.026	0.685 ± 0.003	0.380 ± 0.002
LL MultiLaplace	$\mathbf{0.731 \pm 0.013}$	0.073 ± 0.011	-0.072 ± 0.011	0.941 ± 0.064	0.722 ± 0.008	0.303 ± 0.002
BBB	0.584 ± 0.011	0.268 ± 0.014	-0.268 ± 0.014	2.413 ± 0.126	0.698 ± 0.008	0.353 ± 0.003
MultiBBB	0.621 ± 0.014	0.114 ± 0.016	-0.114 ± 0.016	1.411 ± 0.105	0.757 ± 0.010	0.247 ± 0.009
Rank1-VI	0.673 ± 0.016	0.028 ± 0.010	-0.024 ± 0.014	1.010 ± 0.056	0.719 ± 0.013	0.262 ± 0.010
iVON	0.617 ± 0.011	0.086 ± 0.006	-0.086 ± 0.006	1.201 ± 0.061	0.678 ± 0.008	0.290 ± 0.007
MultiiVON	0.657 ± 0.012	$\mathbf{0.025 \pm 0.005}$	$\mathbf{0.000 \pm 0.009}$	0.998 ± 0.047	0.752 ± 0.012	0.224 ± 0.006
SVGD	0.666 ± 0.004	0.117 ± 0.009	-0.117 ± 0.009	1.557 ± 0.043	0.742 ± 0.007	0.286 ± 0.002
SNGP	0.657 ± 0.006	0.084 ± 0.007	-0.017 ± 0.008	1.256 ± 0.022	0.681 ± 0.008	0.353 ± 0.005
HMC	0.592	0.055	-0.054	1.225	1.000	0.000

(d) Corruption Level 5

Table 8: CIFAR-10: Detailed results on the standard evaluation split and the corruption levels 1, 3, and 5 of CIFAR-10-C.

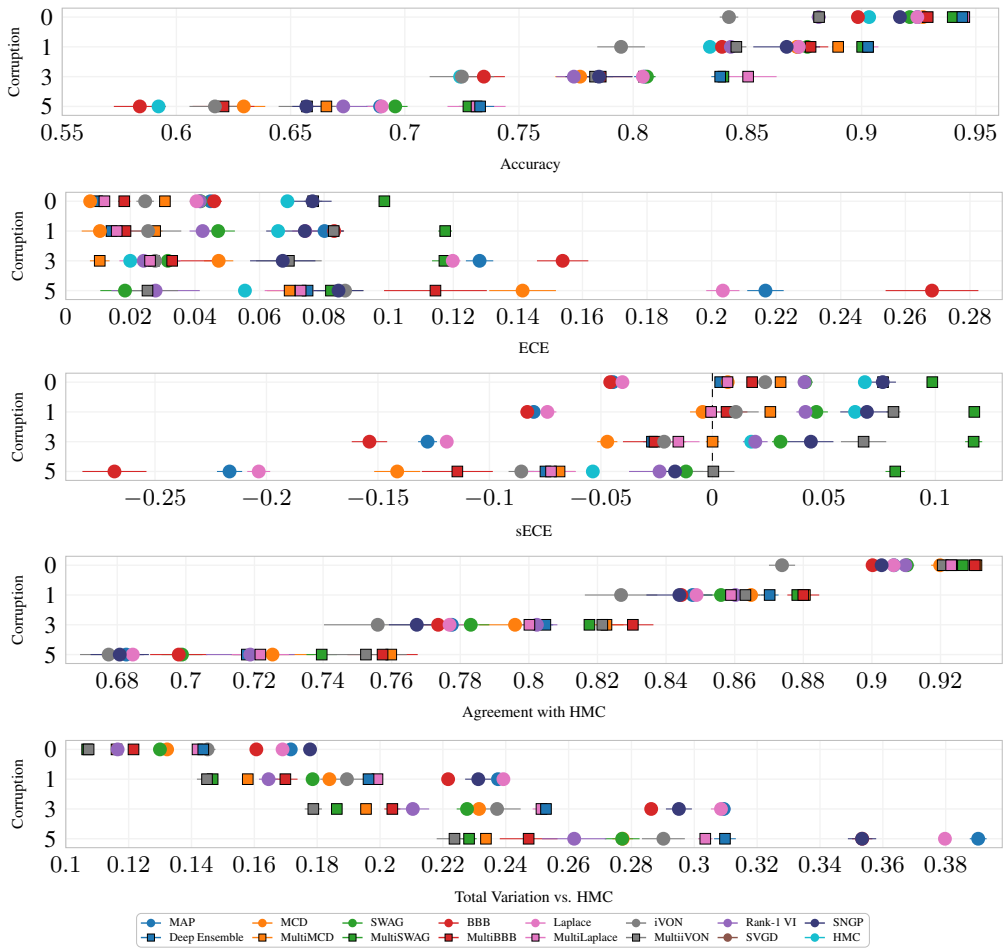

Figure 9: CIFAR-10-(C): All results for the corruption intensities 0, 1, 3, and 5. The corruption intensities are denoted on the y-axis. A negative sECE indicates overconfidence, a positive sECE indicates underconfidence. The plot for the TV is repeated from Figure 5.

G.3 WILDS

We strictly follow the training and evaluation protocol of Koh et al. [47] by reusing their data folds for training, validation, and testing. We use the hyperparameters proposed by Koh et al. [47] where applicable, and set the other hyperparameters to standard values as suggested by the developers of the respective algorithms. If the standard values lead to unexpectedly bad results, we tune the hyperparameters through a grid search. Hyperparameter tuning was performed on the i.d. validation and, where available, o.o.d. validation splits, but never on testing splits. In particular, we select the prior precision of iVON through a grid search over the values $1, 10, 100$, and 500 per model architecture. We find the prior precision of iVON to be hard to tune, as iVON frequently diverges for comparatively small prior precisions such as 1 and 10. BBB works always well with the standard unit prior. We also experiment with other priors but find no difference in performance except on RxRx1-WILDS (see Figure 14). BBB and iVON use two Monte Carlo samples during training. See the sections below for the hyperparameters that were chosen on the individual datasets. We use mixed precision training whenever possible. The VI algorithms as well as the Laplace approximations are mostly trained without mixed precision, as this leads to unstable training.

SNGP uses the same learning rate, weight decay, and number of epochs as the other algorithms. Following the recommendations by Liu et al. [54] and the tuning done by Nado et al. [65], we use a spectral normalization factor of 6.0 for the computer vision tasks and 0.95 for the text classification tasks. On the image classification tasks, SNGP performs significantly better when limiting the input

dimension of the Gaussian Process to 128 or 256 instead of using the output dimension of the previous network layer.

We use 10 posterior samples per prediction during evaluation to constrain the computational overhead of the Bayesian algorithms, which is generally sufficient to capture the predictive distribution [72]. Note that our results are not directly comparable to the results of Daxberger et al. [13], as they build their Deep Ensembles and Laplace approximations from the pretrained models provided by Koh et al. [47]. When comparing our results with the best performing algorithms on the WILDS leaderboard, we only consider the algorithms on the "overall leaderboard", i.e. the algorithms that conform to the official submission guidelines of Koh et al. [47].

G.3.1 Camelyon17-WILDS

Following Koh et al. [47], we train a DenseNet-121 [35] with SGD for 5 epochs with a learning rate of 0.001, weight decay 0.01 and momentum 0.9. SWAG collects 30 parameter samples during the last epoch.

G.3.2 PovertyMAP-WILDS

We train a ResNet-18 [32] using the same hyperparameters as Koh et al. [47] where applicable: A learning rate of 10^{-3} and no weight decay. We only train for 100 epochs as all models were converged after that. SWAG collects 30 parameter samples starting at epoch 50. For BBB, we scale the KL divergence down with a factor of 0.2, as this significantly improves the MSE. Rank-1 VI uses an unscaled KL divergence. The ensembles, Rank-1 VI and SVGD use five members/components. We optimize the log likelihood of the training data and represent the aleatoric uncertainty with a fixed standard deviation of 0.1, as this is the value MAP converges to when jointly optimizing the standard deviation and the model's parameters. For the final evaluations, we do not optimize the standard deviation, as this leads to unstable training with the VI algorithms. Following Koh et al. [47], we aggregate all results over the five folds of PovertyMap, with one seed per fold.

As mentioned in the main paper, iVON performs significantly worse than the other algorithms. We conducted a grid search over prior precisions 1, 10, 100 and 500 with a single seed per value, and found that for 1 and 10 iVON diverges, for 100 iVON achieves an o.o.d. Pearson coefficient on the "A" split of 0.21 and for 500 it achieves a Pearson coefficient of 0.25. Most likely due to their underfitting the non-diverged models are comparatively well calibrated with sECEs of -0.21 for a prior precision of 100 and -0.24 for a prior precision of 500.

Log Marginal Likelihood. The log marginal likelihood is commonly used to jointly evaluate the accuracy and calibration of a regression model. On an evaluation dataset $\mathcal{D}'$, the log marginal likelihood (LML) is given by

$$\text{LML} = \log p(\mathcal{D}' \mid \mathcal{D}) = \log \int p(\mathcal{D}' \mid \boldsymbol{\theta}) p(\boldsymbol{\theta} \mid \mathcal{D}) \, \mathrm{d}\boldsymbol{\theta} \approx \log \sum_n p(\mathcal{D}' \mid \boldsymbol{\theta}_n), \tag{14}$$

where the θ_n are samples from the parameter posterior. When only few predictions are available because sampling parameters θ_n or evaluating the likelihood $p(\mathcal{D}' \mid \boldsymbol{\theta}_n)$ is expensive, the LML may become very noisy. We therefore also report the per-sample log marginal likelihood

$$\begin{aligned} \text{psLML} &= \sum_{(\boldsymbol{x}_i, \boldsymbol{y}_i) \in \mathcal{D}'} \log p(\boldsymbol{y}_i \mid \boldsymbol{x}_i, \mathcal{D}) \\ &= \sum_{(\boldsymbol{x}_i, \boldsymbol{y}_i) \in \mathcal{D}'} \log \int p(\boldsymbol{y}_i \mid \boldsymbol{x}_i, \boldsymbol{\theta}) p(\boldsymbol{\theta} \mid \mathcal{D}) \, \mathrm{d}\boldsymbol{\theta} \\ &\approx \sum_{(\boldsymbol{x}_i, \boldsymbol{y}_i) \in \mathcal{D}'} \log \sum_n p(\boldsymbol{y}_i \mid \boldsymbol{x}_i, \boldsymbol{\theta}_n), \end{aligned} \tag{15}$$

which has a lower variance than the LML. We present the results for the LML, the psLML, the urban/rural Pearson coefficient (see Section 5.1), and the sQCE in Figure 10 and Figure 11. Table 9 shows detailed numerical results.

Model	Worst U/R Pearson	psLML	LML	MSE	QCE	sQCE
MAP	$\mathbf{0.487 \pm 0.074}$	-11.945 ± 2.042	$\mathbf{-11.945 \pm 2.042}$	$\mathbf{0.267 \pm 0.041}$	0.382 ± 0.012	-0.382 ± 0.012
Deep Ensemble	$\mathbf{0.520 \pm 0.075}$	-6.126 ± 1.422	$\mathbf{-12.113 \pm 2.074}$	$\mathbf{0.249 \pm 0.043}$	0.283 ± 0.027	-0.283 ± 0.027
MCD	$\mathbf{0.491 \pm 0.079}$	-6.868 ± 1.720	$\mathbf{-12.175 \pm 2.398}$	$\mathbf{0.259 \pm 0.049}$	0.316 ± 0.023	-0.316 ± 0.023
MultiMCD	$\mathbf{0.516 \pm 0.078}$	-5.053 ± 1.518	$\mathbf{-12.290 \pm 2.409}$	$\mathbf{0.253 \pm 0.052}$	0.271 ± 0.035	-0.271 ± 0.035
SWAG	$\mathbf{0.473 \pm 0.078}$	-12.551 ± 1.994	$\mathbf{-12.621 \pm 2.000}$	$\mathbf{0.280 \pm 0.040}$	0.386 ± 0.012	-0.386 ± 0.012
MultiSWAG	$\mathbf{0.512 \pm 0.078}$	-6.010 ± 1.373	$\mathbf{-12.167 \pm 1.989}$	$\mathbf{0.250 \pm 0.042}$	0.280 ± 0.026	-0.280 ± 0.026
LL Laplace	$\mathbf{0.473 \pm 0.072}$	-12.599 ± 2.191	$\mathbf{-12.599 \pm 2.191}$	$\mathbf{0.280 \pm 0.044}$	0.387 ± 0.012	-0.387 ± 0.012
LL MultiLaplace	$\mathbf{0.516 \pm 0.080}$	-5.614 ± 1.271	$\mathbf{-12.324 \pm 2.141}$	$\mathbf{0.251 \pm 0.044}$	0.265 ± 0.026	-0.265 ± 0.026
BBB	$\mathbf{0.500 \pm 0.072}$	-7.881 ± 2.290	$\mathbf{-12.075 \pm 2.470}$	$\mathbf{0.264 \pm 0.054}$	0.333 ± 0.036	-0.333 ± 0.036
MultiBBB	$\mathbf{0.518 \pm 0.074}$	-6.257 ± 1.462	$\mathbf{-11.498 \pm 2.299}$	$\mathbf{0.252 \pm 0.048}$	0.309 ± 0.027	-0.309 ± 0.027
Rank-1 VI	$\mathbf{0.509 \pm 0.069}$	$\mathbf{-3.568 \pm 1.053}$	$\mathbf{-13.276 \pm 1.978}$	$\mathbf{0.246 \pm 0.043}$	$\mathbf{0.212 \pm 0.028}$	$\mathbf{-0.212 \pm 0.028}$
iVON	$0.249 \pm -$	$-4.657 \pm -$	$-19.787 \pm -$	$0.347 \pm -$	$0.236 \pm -$	$-0.236 \pm -$
SVGD	$\mathbf{0.497 \pm 0.070}$	-5.416 ± 1.270	$\mathbf{-12.524 \pm 2.224}$	$\mathbf{0.254 \pm 0.041}$	0.255 ± 0.026	-0.255 ± 0.026
SNGP	$\mathbf{0.456 \pm 0.072}$	-12.688 ± 1.556	$\mathbf{-12.688 \pm 1.556}$	$\mathbf{0.281 \pm 0.031}$	0.357 ± 0.009	-0.357 ± 0.009

(a) O.o.d. Evaluation Split

Model	Worst U/R Pearson	psLML	LML	MSE	QCE	sQCE
MAP	0.673 ± 0.019	-7.445 ± 0.761	$\mathbf{-7.445 \pm 0.761}$	0.177 ± 0.015	0.348 ± 0.008	-0.348 ± 0.008
Deep Ensemble	$\mathbf{0.703 \pm 0.022}$	-3.438 ± 0.569	$\mathbf{-7.093 \pm 0.744}$	$\mathbf{0.155 \pm 0.014}$	0.228 ± 0.010	-0.228 ± 0.010
MCD	$\mathbf{0.695 \pm 0.010}$	-3.604 ± 0.483	$\mathbf{-7.237 \pm 0.673}$	$\mathbf{0.162 \pm 0.012}$	0.267 ± 0.014	-0.267 ± 0.014
MultiMCD	$\mathbf{0.711 \pm 0.024}$	-2.680 ± 0.358	$\mathbf{-7.383 \pm 0.615}$	$\mathbf{0.156 \pm 0.012}$	0.220 ± 0.014	-0.220 ± 0.014
SWAG	0.664 ± 0.021	-7.719 ± 0.716	$\mathbf{-7.752 \pm 0.723}$	0.183 ± 0.014	0.355 ± 0.003	-0.355 ± 0.003
MultiSWAG	$\mathbf{0.705 \pm 0.023}$	-3.331 ± 0.439	$\mathbf{-7.221 \pm 0.625}$	$\mathbf{0.155 \pm 0.012}$	0.223 ± 0.008	-0.223 ± 0.008
LL Laplace	0.664 ± 0.018	-7.823 ± 0.737	$\mathbf{-7.823 \pm 0.737}$	0.184 ± 0.015	0.357 ± 0.006	-0.357 ± 0.006
LL MultiLaplace	$\mathbf{0.702 \pm 0.023}$	-3.234 ± 0.539	$\mathbf{-7.474 \pm 0.828}$	$\mathbf{0.157 \pm 0.014}$	0.206 ± 0.004	-0.206 ± 0.004
BBB	0.680 ± 0.019	-4.508 ± 0.269	$\mathbf{-7.224 \pm 0.754}$	0.169 ± 0.014	0.286 ± 0.014	-0.286 ± 0.014
MultiBBB	$\mathbf{0.694 \pm 0.014}$	-3.619 ± 0.344	$\mathbf{-7.159 \pm 0.586}$	$\mathbf{0.161 \pm 0.011}$	0.256 ± 0.012	-0.256 ± 0.012
Rank-1 VI	0.669 ± 0.011	$\mathbf{-2.077 \pm 0.323}$	-9.630 ± 1.166	0.173 ± 0.016	$\mathbf{0.162 \pm 0.016}$	$\mathbf{-0.162 \pm 0.016}$
iVON	$0.571 \pm -$	$-3.888 \pm -$	$-15.832 \pm -$	$0.284 \pm -$	$0.201 \pm -$	$-0.201 \pm -$
SVGD	$\mathbf{0.694 \pm 0.026}$	-3.057 ± 0.611	$\mathbf{-7.564 \pm 1.017}$	$\mathbf{0.159 \pm 0.018}$	0.200 ± 0.008	-0.200 ± 0.008
SNGP	$\mathbf{0.692 \pm 0.013}$	-7.135 ± 0.639	$\mathbf{-7.135 \pm 0.639}$	0.170 ± 0.013	0.300 ± 0.008	-0.300 ± 0.008

(b) I.d. Evaluation Split

Table 9: POVERTYMAP-WILDS: Detailed results on the evaluation splits. iVON underperforms, with a Pearson coefficient of 0.249 on the o.o.d. split and a Pearson coefficient of 0.571 on the i.d. split. All models achieve the same LML and MSE within a 95% confidence interval.

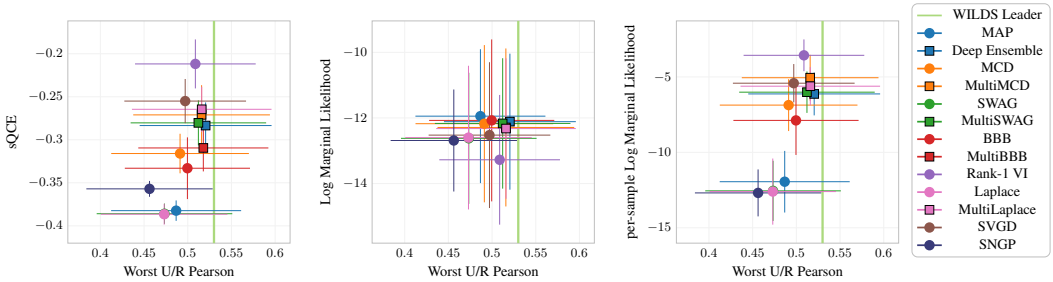

Figure 10: POVERTYMAP-WILDS: Worst urban/rural Pearson coefficient vs. sQCE, LML, and psLML on the o.o.d. evaluation split. Ensemble-based models consistently outperform single-mode models (note that Rank-1 VI's components and SVGD's particles give them ensemble-like properties). The psLML is less noisy than the LML and results in a ranking of the algorithms that is more consistent with the sQCE and the Pearson coefficient. Laplace and SWAG perform nearly equivalently, therefore the data points of SWAG are hidden behind the data points of Laplace. iVON performs significantly worse than the other algorithms and is therefore excluded.

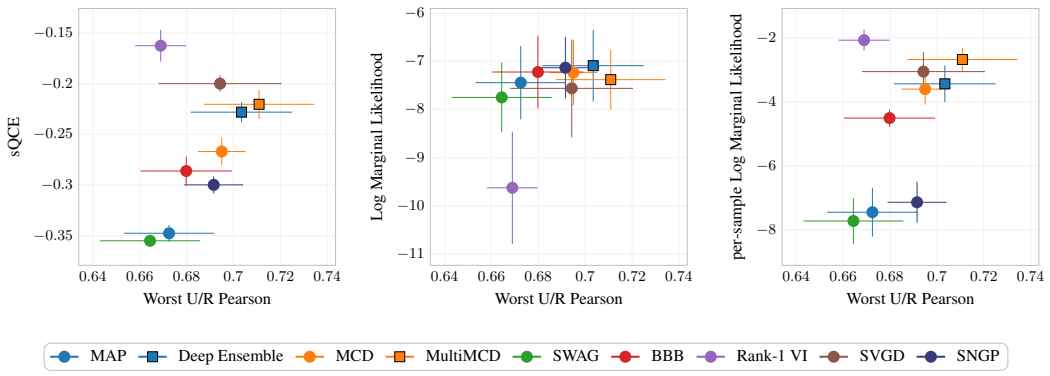

Figure 11: POVERTYMAP-WILDS: Worst urban/rural pearson coefficient vs. sQCE, LML and psLML on the i.d. evaluation split. The WILDS leaderboard [46] does not report the i.d. pearson coefficient.

G.3.3 IWILDCAM-WILDS

Following Koh et al. [47], we finetune a ResNet-50 [32], pretrained on ImageNet [14], for 12 epochs with the Adam optimizer [43]. For each model, we replace the linear classification layer of the ResNet-50 by a randomly initialized one of the appropriate output dimension. We use the hyperparameters that Koh et al. [47] found to work best based on their grid search: A learning rate of $3 \cdot 10^{-5}$ and no weight decay. For MCD, we try dropout rates of 0.1 and 0.2 and select 0.1 due to a slightly better macro F1 score on the evaluation split. iVON uses a prior precision of 100, as optimized by a grid search. We use three seeds per model and build all ensembles by training six models independently and leaving out a different model for each of the three evaluation runs. Figure 12 shows the results on the o.o.d. evaluation split that are not presented in the main paper. Table 10 displays detailed numerical results on the o.o.d. evaluation split and on the i.d. validation split.

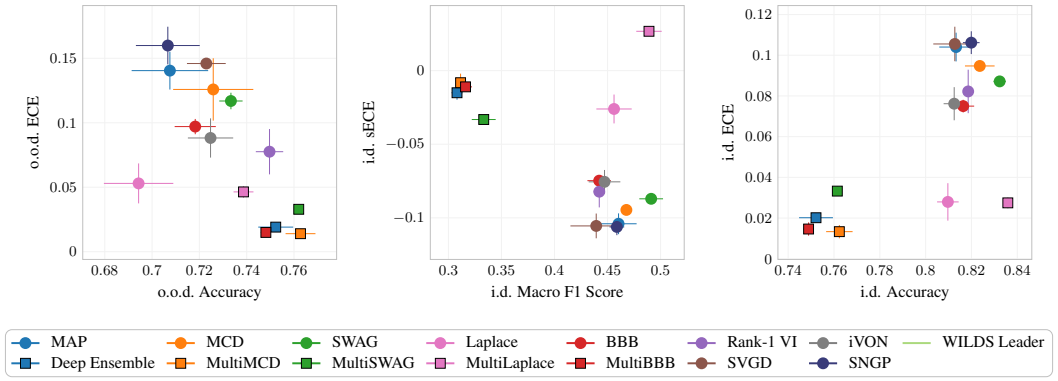

Figure 12: IWILDCAM-WILDS: Macro F1 score, accuracy, sECE and ECE on the o.o.d. evaluation split and the i.d. validation split (see Figure 2a for Macro F1 vs. sECE on the o.o.d. evaluation split). MultiX is less accurate than single-mode approximations on the i.d. split, but better calibrated.

Model	Macro F1 Score	Accuracy	ECE	sECE	NLL
MAP	0.280 ± 0.020	0.708 ± 0.016	0.140 ± 0.015	-0.140 ± 0.015	1.514 ± 0.094
Deep Ensemble	0.312 ± 0.007	0.752 ± 0.007	0.019 ± 0.002	$\mathbf{-0.015 \pm 0.005}$	1.068 ± 0.016
MCD	0.274 ± 0.024	0.710 ± 0.021	0.138 ± 0.013	-0.138 ± 0.013	1.461 ± 0.074
MultiMCD	0.316 ± 0.012	$\mathbf{0.763 \pm 0.006}$	$\mathbf{0.014 \pm 0.004}$	$\mathbf{-0.008 \pm 0.007}$	1.026 ± 0.012
SWAG	0.302 ± 0.009	0.733 ± 0.005	0.117 ± 0.006	-0.117 ± 0.006	1.317 ± 0.032
MultiSWAG	$\mathbf{0.337 \pm 0.005}$	$\mathbf{0.762 \pm 0.001}$	0.033 ± 0.001	-0.033 ± 0.001	$\mathbf{1.009 \pm 0.001}$
LL SWAG	0.294 ± 0.033	0.721 ± 0.023	0.104 ± 0.019	-0.104 ± 0.020	1.295 ± 0.091
LL Laplace	0.270 ± 0.010	0.694 ± 0.015	0.053 ± 0.015	-0.052 ± 0.017	1.567 ± 0.083
LL MultiLaplace	0.304 ± 0.007	0.739 ± 0.004	0.046 ± 0.005	0.046 ± 0.005	1.197 ± 0.012
LL BBB	0.282 ± 0.011	0.718 ± 0.009	0.097 ± 0.006	-0.093 ± 0.005	1.543 ± 0.054
LL MultiBBB	0.312 ± 0.008	0.748 ± 0.002	$\mathbf{0.015 \pm 0.003}$	$\mathbf{-0.012 \pm 0.002}$	1.164 ± 0.011
Rank-1 VI	0.265 ± 0.009	0.750 ± 0.006	0.078 ± 0.018	-0.076 ± 0.017	1.198 ± 0.043
LL iVON	0.265 ± 0.009	0.725 ± 0.010	0.088 ± 0.015	-0.084 ± 0.014	1.331 ± 0.049
LL MultiiVON	0.299 ± 0.006	$\mathbf{0.763 \pm 0.003}$	0.019 ± 0.001	$\mathbf{0.011 \pm 0.003}$	1.036 ± 0.006
SVGD	0.260 ± 0.022	0.723 ± 0.008	0.146 ± 0.004	-0.146 ± 0.004	1.619 ± 0.017
LL SVGD	0.265 ± 0.018	0.737 ± 0.014	0.118 ± 0.003	-0.117 ± 0.003	1.447 ± 0.045
SNGP	0.275 ± 0.010	0.707 ± 0.013	0.160 ± 0.015	-0.160 ± 0.015	1.459 ± 0.095

(a) O.o.d. Test Split

Model	Macro F1 Score	Accuracy	ECE	sECE	NLL
MAP	0.460 ± 0.017	0.813 ± 0.007	0.104 ± 0.007	-0.104 ± 0.007	1.121 ± 0.087
Deep Ensemble	0.308 ± 0.005	0.752 ± 0.007	0.020 ± 0.001	-0.015 ± 0.005	1.067 ± 0.012
MCD	0.457 ± 0.010	0.814 ± 0.002	0.100 ± 0.011	-0.100 ± 0.011	1.105 ± 0.041
MultiMCD	0.311 ± 0.001	0.762 ± 0.006	$\mathbf{0.013 \pm 0.003}$	$\mathbf{-0.008 \pm 0.006}$	1.024 ± 0.016
SWAG	$\mathbf{0.491 \pm 0.011}$	0.832 ± 0.003	0.087 ± 0.002	-0.087 ± 0.002	0.987 ± 0.015
MultiSWAG	0.333 ± 0.011	0.761 ± 0.002	0.033 ± 0.002	-0.033 ± 0.002	1.008 ± 0.002
LL SWAG	0.465 ± 0.043	0.819 ± 0.016	0.088 ± 0.012	-0.088 ± 0.012	1.012 ± 0.060
LL Laplace	0.456 ± 0.017	0.810 ± 0.005	0.028 ± 0.009	-0.026 ± 0.010	1.045 ± 0.058
LL MultiLaplace	$\mathbf{0.489 \pm 0.012}$	$\mathbf{0.836 \pm 0.001}$	0.027 ± 0.003	0.027 ± 0.003	$\mathbf{0.839 \pm 0.012}$
LL BBB	0.442 ± 0.011	0.816 ± 0.005	0.075 ± 0.003	-0.075 ± 0.003	1.143 ± 0.030
LL MultiBBB	0.316 ± 0.006	0.749 ± 0.002	$\mathbf{0.015 \pm 0.003}$	$\mathbf{-0.011 \pm 0.003}$	1.165 ± 0.009
Rank-1 VI	0.442 ± 0.005	0.819 ± 0.001	0.082 ± 0.011	-0.082 ± 0.011	0.960 ± 0.052
LL iVON	0.447 ± 0.015	0.812 ± 0.005	0.076 ± 0.008	-0.076 ± 0.008	1.002 ± 0.028
LL MultiiVON	0.294 ± 0.004	0.763 ± 0.003	0.019 ± 0.003	$\mathbf{0.010 \pm 0.003}$	1.035 ± 0.005
SVGD	0.439 ± 0.024	0.813 ± 0.009	0.106 ± 0.008	-0.105 ± 0.008	1.303 ± 0.136
LL SVGD	0.453 ± 0.018	0.822 ± 0.012	0.094 ± 0.010	-0.094 ± 0.009	1.135 ± 0.234
SNGP	0.459 ± 0.007	0.820 ± 0.004	0.106 ± 0.006	-0.106 ± 0.006	1.081 ± 0.048

(b) I.d. Validation Split

Table 10: iWildCam-wilds: Detailed results on the evaluation splits. LL = Last-Layer. For the MultiX models, the entire model is ensembled.

G.3.4 FMoW-wilds

Following Koh et al. [47], we finetune a DenseNet-121 [35], pretrained on ImageNet [14], for 50 epochs with the Adam optimizer [43] with a batch size of 64 and a learning rate of 10^{-4} that decays by a factor of 0.96 per epoch. For each model, we replace the linear classification layer of the DenseNet-121 by a randomly initialized one of the appropriate output dimension. iVON uses a prior precision of 100. We use five seeds per model and build all ensembles by training six models independently and leaving out a different model for each of the five evaluation runs.

We report in the main paper that the Laplace approximation underfits, with a worst-region accuracy of 0.217 ± 0.012 and sECE of -0.583 ± 0.015 on the o.o.d. test split. Similarly, MultiLaplace only achieves a worst-region accuracy of 0.301 ± 0.004 and sECE of 0.123 ± 0.004 on the o.o.d. evaluation split. The accuracy doesn't change when using 100 posterior samples during evaluation, but increases to 0.243 for 1000 posterior samples. However, using so many samples incurs a significant computational overhead. Note that the better results of Daxberger et al. [13] are most likely due to their usage of models pretrained with ERM. Figure 13 shows additional results for the other models across all regions on the o.o.d. evaluation split, as well as the ECE on the worst region.

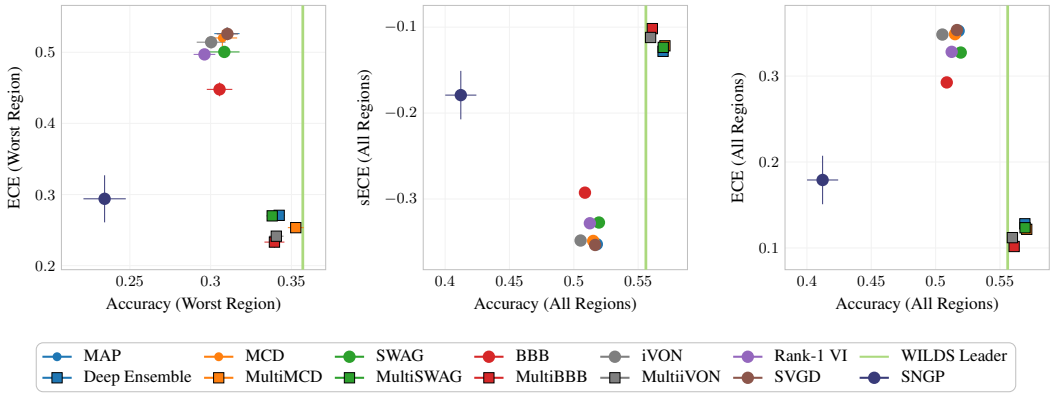

Figure 13: FMoW-WILDS: Accuracy, sECE and ECE on the o.o.d. evaluation split for the region with the lowest accuracy and across all regions (see Figure 2b for accuracy vs. sECE on the worst region). All models are underconfident when evaluated across all regions, but MultiX is less underconfident.

Model	WR Accuracy	WR ECE	WR sECE	WR NLL	Avg Accuracy	Avg ECE	Avg sECE	Avg NLL
MAP	0.310 ± 0.008	0.526 ± 0.009	-0.526 ± 0.009	5.439 ± 0.117	0.518 ± 0.003	0.353 ± 0.002	-0.353 ± 0.002	3.503 ± 0.025
Deep Ensemble	0.342 ± 0.003	0.271 ± 0.004	-0.271 ± 0.004	3.446 ± 0.007	0.569 ± 0.001	0.128 ± 0.001	-0.128 ± 0.001	2.141 ± 0.006
MCD	0.307 ± 0.009	0.520 ± 0.011	-0.520 ± 0.011	5.400 ± 0.118	0.515 ± 0.002	0.349 ± 0.004	-0.349 ± 0.004	3.489 ± 0.036
MultiMCD	$\mathbf{0.353 \pm 0.005}$	0.253 ± 0.005	-0.253 ± 0.005	3.477 ± 0.030	$\mathbf{0.571 \pm 0.000}$	0.122 ± 0.001	-0.122 ± 0.001	2.150 ± 0.007
SWAG	0.308 ± 0.009	0.501 ± 0.007	-0.500 ± 0.007	4.913 ± 0.074	0.520 ± 0.003	0.327 ± 0.003	-0.327 ± 0.003	3.150 ± 0.035
MultiSWAG	0.338 ± 0.003	0.270 ± 0.003	-0.270 ± 0.003	3.243 ± 0.016	0.570 ± 0.001	0.124 ± 0.001	-0.124 ± 0.001	$\mathbf{2.016 \pm 0.008}$
LL SWAG	0.305 ± 0.005	0.516 ± 0.003	-0.516 ± 0.003	5.085 ± 0.036	0.516 ± 0.003	0.343 ± 0.003	-0.343 ± 0.003	3.271 ± 0.028
LL Laplace	0.212 ± 0.008	0.590 ± 0.009	-0.590 ± 0.009	8.249 ± 0.435	0.371 ± 0.014	0.449 ± 0.012	-0.449 ± 0.012	5.947 ± 0.320
LL Laplace (100 Samples)	0.213 ± 0.006	0.588 ± 0.008	-0.588 ± 0.008	8.246 ± 0.355	0.369 ± 0.012	0.449 ± 0.010	-0.449 ± 0.010	5.953 ± 0.262
LL MultiLaplace	0.301 ± 0.004	$\mathbf{0.123 \pm 0.004}$	$\mathbf{-0.123 \pm 0.004}$	4.086 ± 0.047	0.517 ± 0.002	$\mathbf{0.059 \pm 0.002}$	$\mathbf{0.020 \pm 0.002}$	2.744 ± 0.017
LL MultiLaplace (100 Samples)	0.301 ± 0.003	$\mathbf{0.123 \pm 0.003}$	$\mathbf{-0.123 \pm 0.003}$	4.088 ± 0.039	0.517 ± 0.002	$\mathbf{0.059 \pm 0.002}$	$\mathbf{0.020 \pm 0.002}$	2.748 ± 0.016
LL BBB	0.306 ± 0.008	0.448 ± 0.010	-0.448 ± 0.010	6.674 ± 0.343	0.509 ± 0.003	0.293 ± 0.003	-0.293 ± 0.003	4.251 ± 0.053
LL MultiBBB	0.339 ± 0.006	0.233 ± 0.008	-0.233 ± 0.008	4.174 ± 0.085	0.561 ± 0.001	0.102 ± 0.001	-0.102 ± 0.001	2.617 ± 0.008
Rank-1 VI	0.296 ± 0.007	0.497 ± 0.004	-0.497 ± 0.004	4.645 ± 0.147	0.512 ± 0.003	0.328 ± 0.003	-0.328 ± 0.003	2.995 ± 0.037
LL iVON	0.300 ± 0.009	0.514 ± 0.009	-0.514 ± 0.009	4.557 ± 0.112	0.505 ± 0.003	0.348 ± 0.002	-0.348 ± 0.002	3.107 ± 0.023
LL MultiiVON	0.341 ± 0.004	0.241 ± 0.004	-0.241 ± 0.004	$\mathbf{3.177 \pm 0.023}$	0.560 ± 0.001	0.112 ± 0.002	-0.112 ± 0.002	2.060 ± 0.009
SVGD	0.310 ± 0.007	0.526 ± 0.009	-0.526 ± 0.009	5.542 ± 0.083	0.517 ± 0.004	0.354 ± 0.003	-0.354 ± 0.003	3.559 ± 0.041
SNGP	0.234 ± 0.013	0.294 ± 0.033	-0.294 ± 0.033	3.419 ± 0.201	0.412 ± 0.012	0.179 ± 0.028	-0.179 ± 0.028	2.473 ± 0.126

Table 11: FMoW-WILDS: Detailed results on the o.o.d. evaluation split on the worst region as measured by the accuracy on each region and across all regions. For the MultiX models, the entire model is ensembled, but the single-mode approximation is only applied to the classification head. WR = Worst Region, LL = Last-Layer.

G.3.5 RxRx1-WILDS

Following Koh et al. [47], we finetune a ResNet-50 [32], pretrained on ImageNet [14], for 90 epochs with the Adam optimizer [43]. For each model, we replace the linear classification layer of the ResNet-50 by a randomly initialized one of the appropriate output dimension. Following Koh et al. [47], we use a learning rate of 10^{-4} and weight decay 10^{-5}. For MCD, we try dropout rates of 0.1 and 0.2 and select 0.1 due to a slightly better accuracy on the evaluation split. iVON uses a prior precision of 100 as optimized by a grid search. We use five seeds per model and build all ensembles by training six models independently and leaving out a different model for each of the five evaluation runs.

Similar to FMoW, Laplace underperforms accuracy-wise compared to the non-VI algorithms. While we do find a significant increase in accuracy to 0.061 ± 0.002 when using 100 posterior samples, Laplace still performs worse than even MAP. However, Laplace is better calibrated with an sECE of -0.028 ± 0.001.

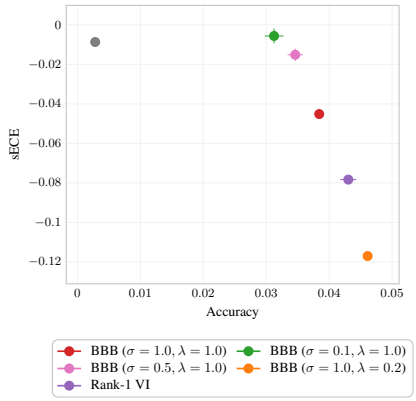

Figure 14: RXRX1-WILDS: BBB and Rank-1 VI under different prior variances σ and posterior temperatures λ. We multiply λ to the KL divergence in the ELBO during training to reduce the regularization strength. However, neither small prior variances nor colder posteriors make BBB competitive with the non-VI algorithms.

Model	i.d. Accuracy	i.d. ECE	i.d. sECE	i.d. NLL	o.o.d. Accuracy	o.o.d. ECE	o.o.d. sECE	o.o.d. NLL
MAP	0.105 ± 0.002	0.232 ± 0.015	-0.232 ± 0.015	6.669 ± 0.121	0.083 ± 0.001	0.262 ± 0.015	-0.262 ± 0.015	7.197 ± 0.149
Deep Ensemble	0.156 ± 0.001	0.066 ± 0.001	-0.026 ± 0.002	$\mathbf{5.211 \pm 0.012}$	0.122 ± 0.000	0.071 ± 0.001	-0.061 ± 0.002	$\mathbf{5.677 \pm 0.019}$
MCD	0.106 ± 0.001	0.257 ± 0.003	-0.257 ± 0.003	6.924 ± 0.035	0.083 ± 0.001	0.288 ± 0.004	-0.288 ± 0.004	7.503 ± 0.043
MultiMCD	0.158 ± 0.001	0.069 ± 0.001	-0.035 ± 0.001	5.327 ± 0.003	0.121 ± 0.000	0.081 ± 0.001	-0.073 ± 0.000	5.836 ± 0.008
SWAG	0.110 ± 0.001	0.269 ± 0.009	-0.269 ± 0.009	6.947 ± 0.088	0.086 ± 0.001	0.301 ± 0.010	-0.301 ± 0.010	7.549 ± 0.109
MultiSWAG	$\mathbf{0.161 \pm 0.001}$	0.075 ± 0.002	-0.042 ± 0.001	5.299 ± 0.009	$\mathbf{0.126 \pm 0.001}$	0.085 ± 0.001	-0.078 ± 0.001	5.824 ± 0.017
LL Laplace	0.012 ± 0.001	0.097 ± 0.001	-0.097 ± 0.001	15.280 ± 0.546	0.010 ± 0.001	0.099 ± 0.001	-0.099 ± 0.001	15.890 ± 0.579
LL Laplace (100 Samples)	0.077 ± 0.000	0.034 ± 0.004	-0.011 ± 0.009	6.624 ± 0.206	0.061 ± 0.002	0.037 ± 0.007	-0.028 ± 0.007	6.909 ± 0.271
LL BBB ($\sigma = 1.0, \lambda = 1.0$)	0.046 ± 0.001	0.032 ± 0.002	-0.032 ± 0.002	6.657 ± 0.019	0.038 ± 0.000	0.045 ± 0.002	-0.045 ± 0.002	6.837 ± 0.012
LL BBB ($\sigma = 0.5, \lambda = 1.0$)	0.040 ± 0.001	$\mathbf{0.007 \pm 0.002}$	$\mathbf{-0.006 \pm 0.003}$	6.632 ± 0.017	0.035 ± 0.001	0.015 ± 0.003	-0.015 ± 0.003	6.737 ± 0.015
LL BBB ($\sigma = 0.1, \lambda = 1.0$)	0.036 ± 0.002	0.010 ± 0.001	$\mathbf{0.003 \pm 0.004}$	6.618 ± 0.017	0.031 ± 0.001	$\mathbf{0.008 \pm 0.002}$	$\mathbf{-0.006 \pm 0.004}$	6.681 ± 0.020
LL BBB ($\sigma = 1.0, \lambda = 0.2$)	0.054 ± 0.001	0.102 ± 0.002	-0.102 ± 0.002	7.598 ± 0.044	0.046 ± 0.001	0.117 ± 0.002	-0.117 ± 0.002	7.957 ± 0.050
Rank-1 VI	0.053 ± 0.001	0.068 ± 0.001	-0.068 ± 0.001	7.389 ± 0.023	0.043 ± 0.001	0.078 ± 0.000	-0.078 ± 0.000	7.577 ± 0.014
LL iVON	0.003 ± 0.000	$\mathbf{0.008 \pm 0.000}$	-0.008 ± 0.000	7.176 ± 0.012	0.003 ± 0.000	$\mathbf{0.009 \pm 0.001}$	$\mathbf{-0.009 \pm 0.001}$	7.213 ± 0.013
SVGD	0.102 ± 0.001	0.354 ± 0.005	-0.354 ± 0.005	8.254 ± 0.080	0.081 ± 0.002	0.382 ± 0.005	-0.382 ± 0.005	8.936 ± 0.088
SNGP	0.089 ± 0.006	0.245 ± 0.023	-0.245 ± 0.023	6.588 ± 0.272	0.067 ± 0.005	0.273 ± 0.019	-0.273 ± 0.019	7.070 ± 0.221

Table 12: RXRX1-WILDS: Detailed results on the i.d. and the o.o.d. evaluation split. LL = Last-Layer. For the MultiX models, the entire model is ensembled, but the single-mode approximation is only applied to the classification head. We evaluate multiple hyperparameter combinations for LL BBB, as the standard parameters do not perform well. The failure of VI is equally present with LL BBB, LL Rank-1 VI, and LL iVON.

G.3.6 CIVILCOMMENTS-WILDS

We use the pretrained DistilBERT [76] model from HuggingFace transformers [91] with a classification head consisting of two linear layers with a ReLU nonlinearity and a Dropout unit with a drop rate of 0.2 between them. Following Koh et al. [47], we finetune the pretrained checkpoint with a learning rate of $1 \cdot 10^{-5}$ and, where applicable, a weight decay factor of $1 \cdot 10^{-2}$ for three epochs using the Adam optimizer [43]. SWAG collects ten parameter samples during the last two epochs of training. iVON uses a prior precision of 500, as optimized by a grid search. We use five seeds for all non-ensembled models. The ensembles are build from four of the five single-model versions, leaving out a different member per model to create five different ensembled models of four members each.

We note in the main paper that MCD results in less accurate and more overconfident models. We investigate this further by experimenting with different dropout rates in Figure 15. While a dropout rate of 0.1 had no impact, dropout rates of 0.05 and 0.01 lead to progressively better accuracy and calibration, coming close to MAP. However, there is still no accuracy or calibration benefit to be gained from using MCD.

G.3.7 AMAZON-WILDS

We use the pretrained DistilBERT [76] model from HuggingFace transformers [91] with a classification head consisting of two linear layers with a ReLU nonlinearity and a Dropout unit with a drop rate of 0.2 between them. Following Koh et al. [47], we finetune the pretrained checkpoint with a learning rate of 10^{-5} and, where applicable, a weight decay factor of 10^{-2} using the Adam optimizer [43]. Contrary to Koh et al. [47], we finetune for five epochs, as we find that the validation accuracy

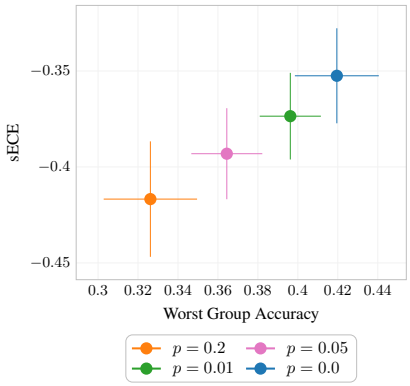

Figure 15: CIVILCOMMENTS-WILDS: Accuracy and sECE for different MCD dropout rates p. While smaller dropout rates improve the accuracy, the models are still less accurate and more overconfident than MAP.

Model	WG Accuracy	WG ECE	WG sECE	WG NLL	Avg Accuracy	Avg ECE	Avg sECE	Avg NLL
MAP	0.420 ± 0.021	0.353 ± 0.025	-0.353 ± 0.025	1.455 ± 0.086	0.916 ± 0.001	0.012 ± 0.003	-0.012 ± 0.003	0.207 ± 0.001
Deep Ensemble	0.419 ± 0.008	0.349 ± 0.010	-0.349 ± 0.010	1.416 ± 0.032	0.916 ± 0.000	0.010 ± 0.001	-0.010 ± 0.001	0.204 ± 0.000
MCD ($p = 0.2$)	0.326 ± 0.023	0.417 ± 0.030	-0.417 ± 0.030	1.391 ± 0.074	0.918 ± 0.000	0.007 ± 0.005	$\mathbf{0.006 \pm 0.006}$	0.204 ± 0.001
MCD ($p = 0.1$)	0.325 ± 0.021	0.418 ± 0.027	-0.418 ± 0.027	1.390 ± 0.070	0.918 ± 0.000	$\mathbf{0.007 \pm 0.005}$	$\mathbf{0.006 \pm 0.005}$	0.204 ± 0.001
MCD ($p = 0.05$)	0.364 ± 0.018	0.393 ± 0.024	-0.393 ± 0.024	1.430 ± 0.065	0.918 ± 0.000	$\mathbf{0.005 \pm 0.002}$	$\mathbf{-0.003 \pm 0.004}$	$\mathbf{0.203 \pm 0.001}$
MCD ($p = 0.01$)	0.396 ± 0.015	0.374 ± 0.023	-0.374 ± 0.023	1.452 ± 0.114	0.917 ± 0.000	0.011 ± 0.003	-0.011 ± 0.003	0.206 ± 0.001
MultiMCD ($p = 0.2$)	0.326 ± 0.005	0.412 ± 0.007	-0.412 ± 0.007	1.363 ± 0.022	0.919 ± 0.000	0.009 ± 0.002	0.009 ± 0.002	$\mathbf{0.203 \pm 0.000}$
SWAG	0.448 ± 0.021	$\mathbf{0.197 \pm 0.041}$	$\mathbf{-0.184 \pm 0.027}$	0.872 ± 0.050	0.877 ± 0.024	0.152 ± 0.024	0.152 ± 0.024	0.396 ± 0.019
MultiSWAG	0.429 ± 0.016	$\mathbf{0.183 \pm 0.018}$	$\mathbf{-0.183 \pm 0.018}$	$\mathbf{0.819 \pm 0.011}$	0.901 ± 0.002	0.184 ± 0.002	0.184 ± 0.002	0.388 ± 0.004
LL Laplace	0.424 ± 0.016	0.348 ± 0.018	-0.347 ± 0.018	1.438 ± 0.065	0.916 ± 0.001	0.011 ± 0.002	-0.011 ± 0.002	0.207 ± 0.001
LL MultiLaplace	0.420 ± 0.008	0.348 ± 0.010	-0.348 ± 0.010	1.411 ± 0.032	0.916 ± 0.000	0.010 ± 0.001	-0.009 ± 0.001	0.204 ± 0.000
LL BBB	$\mathbf{0.537 \pm 0.032}$	0.362 ± 0.032	-0.361 ± 0.033	2.192 ± 0.278	0.918 ± 0.002	0.056 ± 0.002	-0.056 ± 0.002	0.333 ± 0.017
LL MultiBBB	$\mathbf{0.525 \pm 0.012}$	0.338 ± 0.012	-0.338 ± 0.012	1.801 ± 0.078	0.922 ± 0.000	0.041 ± 0.001	-0.041 ± 0.001	0.265 ± 0.003
Rank-1 VI	$\mathbf{0.540 \pm 0.028}$	0.373 ± 0.030	-0.373 ± 0.030	2.065 ± 0.179	0.917 ± 0.002	0.060 ± 0.002	-0.060 ± 0.002	0.319 ± 0.007
LL iVON	0.480 ± 0.045	0.421 ± 0.048	-0.421 ± 0.048	2.198 ± 0.263	0.919 ± 0.003	0.054 ± 0.002	-0.054 ± 0.002	0.299 ± 0.014
LL MultiiVON	0.465 ± 0.011	0.396 ± 0.015	-0.396 ± 0.015	1.752 ± 0.073	$\mathbf{0.924 \pm 0.001}$	0.039 ± 0.001	-0.039 ± 0.001	0.240 ± 0.002
SVGD	0.384 ± 0.068	0.380 ± 0.079	-0.379 ± 0.079	1.393 ± 0.154	0.915 ± 0.003	0.011 ± 0.005	-0.008 ± 0.008	0.208 ± 0.002
SNGP	0.394 ± 0.039	0.388 ± 0.036	-0.388 ± 0.036	1.341 ± 0.078	0.919 ± 0.001	0.014 ± 0.006	-0.014 ± 0.006	0.206 ± 0.004

Figure 16: CIVILCOMMENTS-WILDS: Detailed results on the o.o.d. evaluation split for the worst group (WG, determined by the accuracy on each group) and averaged over all groups. LL = Last-Layer.

is still increasing after three epochs. SWAG collects 30 parameter samples during the last two epochs of training. We also experiment with last-layer versions of SWAG and MCD, but find both to perform very similar to MAP (see Table 13). iVON uses a prior precision of 500, as optimized by a grid search. We use six seeds for all non-ensembled models. The ensembles are build from five of the six single-model versions, leaving out a different member per model to create five different ensembled models of five members each.

Model	o.o.d. 10 Accuracy	o.o.d. Accuracy	o.o.d. ECE	o.o.d. sECE	o.o.d. NLL	i.d. 10 Accuracy	i.d. Avg Accuracy	i.d. ECE	i.d. sECE	i.d. NLL
MAP	0.453 ± 0.010	0.655 ± 0.003	0.067 ± 0.006	-0.067 ± 0.006	0.815 ± 0.007	0.477 ± 0.008	0.678 ± 0.002	0.049 ± 0.007	-0.049 ± 0.007	0.755 ± 0.005
Deep Ensemble	0.453 ± 0.000	0.659 ± 0.001	0.058 ± 0.002	-0.058 ± 0.002	0.800 ± 0.001	0.480 ± 0.000	0.682 ± 0.000	0.040 ± 0.002	-0.040 ± 0.002	0.742 ± 0.001
MCD	0.447 ± 0.013	0.657 ± 0.002	0.020 ± 0.011	-0.019 ± 0.012	0.789 ± 0.004	0.472 ± 0.012	0.678 ± 0.001	0.015 ± 0.006	$\mathbf{-0.002 \pm 0.013}$	0.741 ± 0.003
MultiMCD	0.451 ± 0.005	0.660 ± 0.001	$\mathbf{0.012 \pm 0.003}$	$\mathbf{-0.012 \pm 0.003}$	0.780 ± 0.001	0.475 ± 0.007	0.682 ± 0.000	$\mathbf{0.007 \pm 0.002}$	$\mathbf{0.005 \pm 0.003}$	0.733 ± 0.000
LL MCD	0.451 ± 0.008	0.656 ± 0.003	0.069 ± 0.008	-0.069 ± 0.008	0.816 ± 0.011	0.478 ± 0.011	0.679 ± 0.002	0.051 ± 0.009	-0.051 ± 0.009	0.756 ± 0.009
SWAG	0.436 ± 0.011	0.639 ± 0.006	0.032 ± 0.003	0.031 ± 0.004	0.840 ± 0.014	0.460 ± 0.010	0.658 ± 0.006	0.047 ± 0.004	0.047 ± 0.004	0.807 ± 0.015
MultiSWAG	0.443 ± 0.005	0.646 ± 0.001	0.040 ± 0.001	0.040 ± 0.001	0.828 ± 0.002	0.469 ± 0.005	0.667 ± 0.001	0.057 ± 0.001	0.057 ± 0.001	0.796 ± 0.003
LL SWAG	0.452 ± 0.012	0.656 ± 0.003	0.048 ± 0.009	-0.048 ± 0.009	0.802 ± 0.006	0.474 ± 0.010	0.679 ± 0.002	0.031 ± 0.008	-0.030 ± 0.009	0.747 ± 0.005
LL Laplace	0.455 ± 0.009	0.654 ± 0.003	0.067 ± 0.006	-0.067 ± 0.006	0.816 ± 0.006	0.482 ± 0.009	0.678 ± 0.002	0.048 ± 0.007	-0.048 ± 0.007	0.756 ± 0.004
LL MultiLaplace	0.453 ± 0.000	0.659 ± 0.001	0.058 ± 0.001	-0.058 ± 0.001	0.800 ± 0.001	0.480 ± 0.000	0.682 ± 0.000	0.040 ± 0.002	-0.040 ± 0.002	0.742 ± 0.001
LL BBB	0.527 ± 0.006	0.695 ± 0.007	0.154 ± 0.005	-0.154 ± 0.005	0.898 ± 0.019	0.560 ± 0.000	0.730 ± 0.006	0.128 ± 0.004	-0.128 ± 0.004	0.778 ± 0.015
LL MultiBBB	$\mathbf{0.533 \pm 0.000}$	$\mathbf{0.709 \pm 0.002}$	0.105 ± 0.001	-0.105 ± 0.001	$\mathbf{0.748 \pm 0.001}$	$\mathbf{0.573 \pm 0.000}$	$\mathbf{0.746 \pm 0.001}$	0.079 ± 0.002	-0.079 ± 0.002	$\mathbf{0.648 \pm 0.002}$
Rank-1 VI	0.527 ± 0.005	0.695 ± 0.003	0.173 ± 0.004	-0.173 ± 0.004	0.923 ± 0.015	0.558 ± 0.004	0.729 ± 0.003	0.147 ± 0.004	-0.147 ± 0.004	0.801 ± 0.010
LL iVON	0.458 ± 0.010	0.661 ± 0.002	0.053 ± 0.010	-0.053 ± 0.010	0.794 ± 0.008	0.484 ± 0.009	0.684 ± 0.002	0.037 ± 0.010	-0.037 ± 0.010	0.737 ± 0.006
LL MultiiVON	0.459 ± 0.007	0.665 ± 0.001	0.045 ± 0.002	-0.045 ± 0.002	0.779 ± 0.001	0.484 ± 0.005	0.687 ± 0.001	0.029 ± 0.003	-0.029 ± 0.002	0.724 ± 0.001
SVGD	0.456 ± 0.010	0.661 ± 0.003	0.049 ± 0.005	-0.049 ± 0.005	0.793 ± 0.011	0.477 ± 0.010	0.682 ± 0.002	0.035 ± 0.005	-0.034 ± 0.005	0.740 ± 0.008
SNGP	0.451 ± 0.013	0.661 ± 0.001	0.053 ± 0.008	-0.053 ± 0.008	0.800 ± 0.002	0.487 ± 0.013	0.685 ± 0.001	0.036 ± 0.008	-0.035 ± 0.008	0.737 ± 0.001

Table 13: AMAZON-WILDS: Detailed results on the i.d. and the o.o.d. evaluation splits. LL = Last-Layer.